The upgraded Polaris powder diffractometer at the ISIS neutron source

Review of Scientific Instruments ARTICLE scitation.org/journal/rsi

The upgraded Polaris powder diffractometer at the ISIS neutron source

Cite as: Rev. Sci. Instrum. 90, 115101 (2019); doi: 10.1063/1.5099568
Submitted: 6 July 2019 • Accepted: 11 October 2019 •
Published Online: 1 November 2019

R. I. Smith,[1,a] S. Hull,[1] M. G. Tucker,[1,b] H. Y. Playford,[1] D. J. McPhail,[1] S. P. Waller,[1] and S. T. Norberg[2,c]

AFFILIATIONS

[1]The ISIS Facility, STFC Rutherford Appleton Laboratory, Harwell Campus, Didcot, Oxfordshire OX11 0QX, United Kingdom
[2]Department of Chemistry and Chemical Engineering, Chalmers University of Technology, SE-412 96 Gothenburg, Sweden

[a]**Author to whom correspondence should be addressed:** ron.smith@stfc.ac.uk
[b]**Present address:** Spallation Neutron Source, Oak Ridge National Laboratory, 1 Bethel Valley Road, Oak Ridge, TN 37830, USA.
[c]**Present address:** Pharmaceutical Technology and Development, AstraZeneca, Pepparedsleden 1, 431 83 Mölndal, Sweden.

ABSTRACT

This paper describes the design and operation of the Polaris time-of-flight powder neutron diffractometer at the ISIS pulsed spallation neutron source, Rutherford Appleton Laboratory, UK. Following a major upgrade to the diffractometer in 2010–2011, its detector provision now comprises five large ZnS scintillator-based banks, covering an angular range of $6^\circ \leq 2\theta \leq 168^\circ$, with only minimal gaps between each bank. These detectors have a substantially increased solid angle coverage ($\Omega \sim 5.67$ sr) compared to the previous instrument ($\Omega \sim 0.82$ sr), resulting in increases in count rate of between 2× and 10×, depending on 2θ angle. The benefits arising from the high count rates achieved are illustrated using selected examples of experiments studying small sample volumes and performing rapid, time-resolved investigations. In addition, the enhanced capabilities of the diffractometer in the areas of *in situ* studies (which are facilitated by the installation of a novel design of radial collimator around the sample position and by a complementary programme of advanced sample environment developments) and in total scattering studies (to probe the nature of short-range atomic correlations within disordered crystalline solids) are demonstrated.

I. INTRODUCTION

The neutron diffraction technique is now well established as an essential tool for the characterization of both crystalline and disordered materials, especially in those areas which focus on the intrinsic strengths of the neutron (its use as a bulk probe, sensitivity to magnetic order, sensitivity to light elements, *Q*-independent form factor, etc.). In particular, neutron powder diffraction has made significant contributions to our understanding of many families of high profile materials [high-T_c superconductors,[1] collosal magnetoresistive (CMR) oxides,[2] C_{60},[3] lithium battery materials,[4] molecular ices,[5] etc.] and has been shown to produce consistently more accurate quantitative structure factors than equivalent X-ray methods, mainly due to better powder averaging and the lack of a *Q*-dependent form factor for nuclear scattering. Neutron powder diffraction studies at pulsed spallation sources, such as ISIS in the UK, SNS in the USA, and J-PARC in Japan, offer a number of advantages over their counterparts at steady-state, reactor-based sources (such as the ILL in France, FRM-II in Munich, and OPAL in Australia) in terms of their high flux of epithermal neutrons, fixed scattering geometry, and essentially constant $\Delta d/d$ resolution at a given scattering angle.

In the UK, over the past 30 years, the ISIS spallation neutron source at the STFC's Rutherford Appleton Laboratory has developed a suite of neutron powder diffractometers, which can be classified as either "general purpose" instruments such as HRPD, GEM, and Polaris (to study a diverse range of scientific disciplines, from the "traditional" areas of solid state chemistry, magnetism and structural physics, through to emerging areas such as archeometry, time-resolved studies, and nanostructured materials) or more specialized facilities such as WISH (optimized for diffraction studies of complex magnetic materials), PEARL (for diffraction studies of materials under high hydrostatic pressures), and ENGIN-X (for the application of neutron diffraction methods to probe engineering

components). In the former case, general purpose instruments can be optimized for high resolution (such as HRPD) to study complex materials, multiphase mixtures, and subtle structural distortions or high intensity (such as GEM and Polaris) to allow rapid time-resolved studies, measurements of weak scattering features, and investigations of relatively small samples within complex sample environments.

In the specific case of the Polaris diffractometer, the beamline was originally envisaged as a development facility for neutron polarizing filter devices but was converted to full time use as a powder diffractometer in 1989. Despite a rather modest initial detector complement (42 ^{3}He gas tubes), its potential quickly became apparent in a number of scientific areas.[6] In particular, measurements performed on Polaris demonstrated the importance of epithermal neutrons to collect data at high scattering vectors Q (or, equivalently, low d-spacings) and highlighted how the fixed scattering geometry at a pulsed neutron source could be used to develop specialized sample environment (such as the Paris-Edinburgh pressure cell[7]) and to measure residual stress distributions within engineering components.[8] These advances inevitably led to a rapid increase in the breadth of the scientific programme and a high over-demand for beamtime on Polaris, culminating in the construction of new instruments dedicated to diffraction at high pressures (PEARL) and engineering applications (ENGIN, itself later upgraded to ENGIN-X). ISIS responded by increasing the Polaris detector complement to reduce data collection times and, hence, increase both the experiment throughput and range of experiments undertaken. Over the next ~20 years, Polaris became one of the most productive neutron powder diffractometers in the world (with over 700 publications) but, with significant progress in neutron optics and detector technologies, its performance became inferior to other facilities, including the newer GEM diffractometer at ISIS which was completed in 2005.[9]

Around 2007, and following consultation with its user community, ISIS began a major project to upgrade Polaris, both to meet the exceptionally high user demand and to allow scope for expansion into several new and important areas of solid-state research. A number of key scientific areas were highlighted to guide the specification of the upgraded instrument, including photovoltaics, oxygen conducting ceramics for use in fuel cells, hydrogen storage media, improved Li^+ ion conducting materials for battery applications, morphotropic phase boundaries in doped piezoelectric perovskites (such as PZT), rigid unit vibrational modes within network structures, negative thermal expansion, interactions within "host-guest" systems and catalysts, rapid response gas sensors, nanostructured materials, and *in situ* studies of chemical and electrochemical processes. This process therefore identified a number of key design criteria for the upgraded diffractometer, including the following:

(i) maximize the count rate over a wide range of d-spacings (or scattering vector, Q) via the installation of a large solid angle of detector coverage to provide excellent counting statistics.
(ii) improve the instrumental resolution $\Delta d/d$, especially at backscattering angles where the highest resolution is most easily achieved.
(iii) minimize instrumental backgrounds, including the installation of advanced beam defining jaws in the incident beam and a radial collimator to reduce the amount of spurious scattering from complex sample environment devices which reaches the detectors.

This paper summarizes the design of the upgraded Polaris diffractometer, which is now a state-of-the-art instrument able to fully exploit the excellent characteristics of the ISIS pulsed neutron source. Section II describes the various components of the instrument and is followed by a number of recent scientific examples to illustrate its current performance and future potential.

II. INSTRUMENT DESIGN

Figure 1 shows a schematic overview of the major components of the upgraded Polaris beamline. Each aspect of the design is discussed in more detail in Subsections II A to II H below.

A. Incident beamline

The Polaris powder diffractometer occupies beamline N7 on ISIS Target Station 1, receiving neutrons from an ambient temperature (316 K) H_2O-filled moderator of dimensions 12 cm (width) × 12.5 cm (height) × 4.5 cm (depth). An internal gadolinium "poisoning" foil placed 15 mm from its "front" face [as viewed by beamlines on the north (N) side of the target station] serves to ensure that longer wavelength neutrons maintain a sharp time structure, albeit with a small decrease in neutron flux. To keep beam divergence low and thus provide good resolution, the beamline does not view the whole moderator face and instead only accepts neutrons from approximately the center three-quarters: 8.8 cm (w) × 8.0 cm (h). The incident beam is then tapered down to the

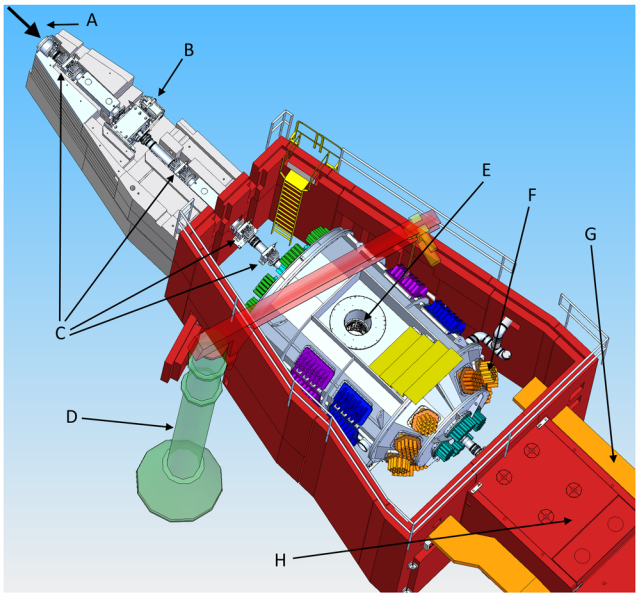

FIG. 1. Schematic diagram showing the layout of the Polaris beamline following its upgrade. A—direction of incident neutron beam from target station, B—t-zero chopper, C–beam defining adjustable jaws, D—crane (for loading sample environment equipment), E—sample position, F—detector module (1 of 38), G—cable routes to electronics cabin, and H—beam stop.

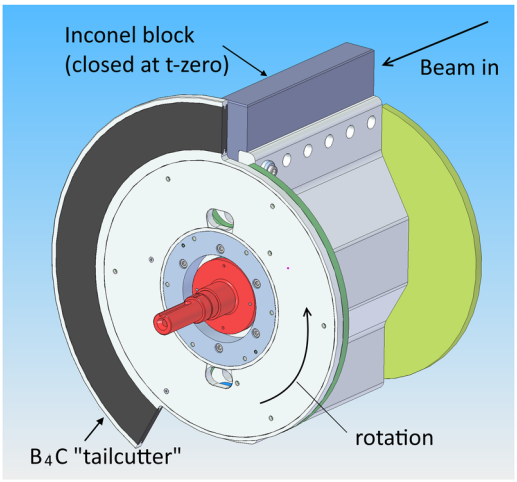

FIG. 2. The neutron chopper installed on the Polaris beamline. The combination of the inconel block and B_4C "tailcutter" significantly reduces the fluxes of fast neutrons and very slow neutrons, respectively.

1.5 cm (w) × 4.0 cm (h) cross section required at the sample position, located 14.0 m from the moderator, by placing a large number of fixed collimating apertures (manufactured from boron-loaded wax, steel shot, and boron carbide) at regular intervals along the beamline. The whole of the incident beamline from the shutter to the detector/sample tank is evacuated in order to minimize attenuation of the neutron beam by air and also to reduce background scattering.

B. Jaws system

In order to enable the neutron beam dimensions at the sample position to be tuned for different sample sizes, an additional series of adjustable collimating jaws are incorporated into the incident beamline. Each collimator unit has 4 independently adjustable sintered B_4C blocks which absorb unwanted neutrons, allowing both the beam size and any required offset at the sample position to be controlled. The first four jaws sets are located in the incident beamline at distances of 6.5 m, 9.4 m, 11.1 m, and 11.7 m from the moderator, whilst a final set is positioned inside the sample tank, ~0.5 m before the sample position, to minimize the beam penumbra. All the jaws sets are driven by stepper motors, with the motors themselves in air but the moving parts in the vacuum of the beamline, and use Renishaw optical encoders and Galil DMC 2280 motion controllers.

C. Inconel (*t*-zero) chopper

A *t*-zero chopper is located at a position 8 m from the moderator (see Fig. 2). For conventional powder diffraction studies, this rotates at 50 Hz in synchronization with the proton pulse from the ISIS accelerator (rotation axis parallel to the beamline) and reduces the instrument background by preventing unwanted neutrons from traveling along the beamline. This is achieved first by a 300 mm thick block of inconel alloy which closes the beamline as the proton beam strikes the ISIS target, preventing the very highest energy neutrons produced from traveling toward the sample position. Once this has moved out of the way, neutrons are allowed past to reach the sample, until a B_4C "tail cutter" closes at around $^2/_3$ of the way through the 20 ms time interval between ISIS pulses to prevent "frame overlap" (where the small number of the very slowest, lowest energy, neutrons are overtaken by the fastest neutrons from the next ISIS pulse, causing data corruption).

For total scattering studies, where data to higher Q (shorter d-spacing/lower time-of-flight) are often required, the chopper may be stopped and parked in an "open" position to allow all neutrons to reach the sample. This will result in slightly higher instrument backgrounds, which can be corrected by collection of appropriate empty instrument, empty sample container, etc., data sets.

D. Beamline monitors

A series of six beamline monitors are incorporated along the beamline, located before and after the chopper and between each of the sets of collimating jaws. The purpose of the first five monitors is primarily diagnostic to confirm the neutron transmission of the chopper and jaws. However, the monitor closest to the sample position is used during data normalization to provide a measure of the neutron flux reaching the sample. A final, seventh, monitor is located in the transmitted neutron beam ~3 m after the sample position and is suitable for, e.g., accurate alignment of collimating pieces around sample containers or transmission measurements. All monitors are of an identical design, shown in Fig. 3, in which a thin vanadium foil sits in the neutron beam and is inclined at 45° to it. This scatters a small proportion of neutrons upward into a piece of ZnS scintillator,

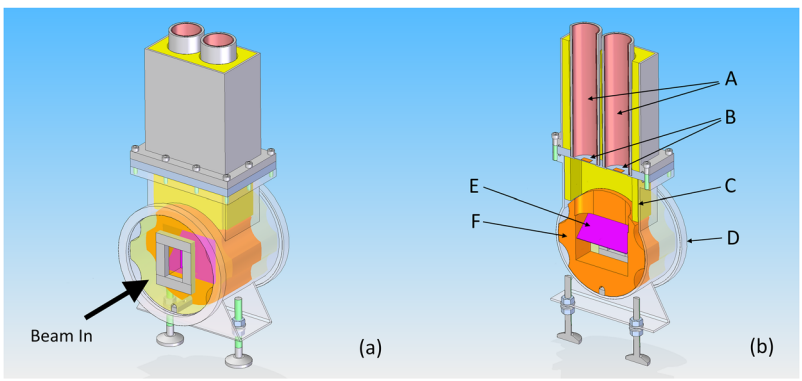

FIG. 3. (a) The incident beam monitor installed on the Polaris beamline and (b) cutaway view showing A—position of photomultiplier tubes, B—thin vacuum window and scintillator, C and F—B_4C shielding, D—incident beam pipe (flight tube), and E—vanadium foil inclined at 45° to the incident neutron beam.

TABLE I. The specifications of the various detector banks of the upgraded Polaris diffractometer.

Detector bank	Number	2θ range (deg)	Secondary flight path[a] (m)	Solid angle (sr)	$\Delta d/d$ resolution (%)	d_{max} (Å)
Very low angle	1	6.7–14.0	2.25	0.26	2.7	>40
Low angle (2 banks)	2	19.5–34.1	2.36–1.31	1.04	1.5	13.5
	3	40.4–66.4	1.57–0.925	0.92	0.85	7.0
90°	4	75.2–112.9	1.08–0.710	1.33	0.51	4.1
Back scattering	5	134.6–167.4	1.54–0.795	2.12	0.30	2.65

[a]Secondary flight path = sample position to detector distance. Primary flight path (moderator to sample position distance) = 14.0 m.

where the photons produced are detected by one of two photomultiplier tubes (PMTs). The efficiency of the monitor is determined by the thickness of the vanadium foil (0.04 mm for "diagnostics" and 0.5 mm for "normalization").

E. Detectors

The $\Delta d/d$ resolution of a time-of-flight neutron powder diffractometer at a pulsed source is a combination of three components which represent uncertainties in the neutron time-of-flight (Δt), flightpath (ΔL), and scattering angle ($\Delta 2\theta$). This resolution, manifest in the width of the peaks, varies dramatically with detector angle, 2θ, and for this reason, the detector elements typically are grouped into a number of discrete banks, with each bank containing elements covering a similar d-spacing range and having a similar $\Delta d/d$ resolution. Detector banks at high 2θ angles have the sharpest Bragg reflections but only measure to relatively low maximum d-spacings, whereas detectors at low 2θ angles have poor resolution (broader reflections) but are able to access much longer d-spacings (see Table I). Being an upgrade to an existing instrument, there were also a number of geometric constraints imposed on detector positioning by, for example, neighboring instruments.

Consequently, the approach taken during the detector design was to use the McStas neutron ray-trace simulation package[10] to perform a large number of Monte Carlo simulations of individual detectors over a grid of positions within the available space to determine their expected resolution (see Fig. 4). From these results, optimum loci of approximately constant $\Delta d/d$ along which to place the active areas of the detector modules were selected in such a way that also maximized the solid angle of detector coverage (and, hence, countrate).

The final detector complement on Polaris comprises 38 individual detector modules, grouped into five discrete banks (see Fig. 5), which are all based on ZnS:Ag/^{6}LiF scintillators. Each detector bank has its own design of module(s), consisting of between 40 and 110 individual detector elements (pixels), each 5 mm wide and arranged so that they follow closely the curved Debye-Scherrer geometry of diffraction. The neutron detection efficiency of the scintillator is ~50% at a neutron wavelength of 1 Å, with good neutron/gamma discrimination. Behind these elements, 1 mm diameter fiber optic light guides on a 2 mm pitch transmit the scintillator output to photomultiplier tubes (PMTs), where the light is converted to an electric charge. In order to reduce the total number of PMTs and electronics channels required, the fiber optic light guides are arranged such that any one detector element is coded to a unique pair of PMTs such that a simultaneous signal in two PMT channels can be used to determine where on the detector the event occurred.

In total, the upgraded Polaris detector array contains 2954 individual detector elements, more than 450 km of fiber optic light guide and 924 PMTs. The specification for each of the five detector banks is given in Table I.

F. Sample tank

Conventionally, time-of-flight neutron diffractometers are built such that the sample is placed in an evacuated sample tank

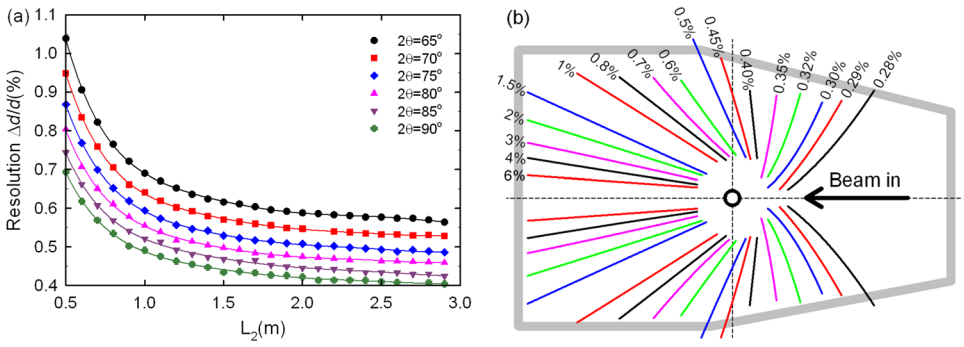

FIG. 4. Results of the McStas simulations of the $\Delta d/d$ resolution achievable on Polaris. The data obtained as a function of secondary flightpath at different scattering angles (a) is used to generate loci of constant $\Delta d/d$ resolution (b). The latter are used to guide the layout of individual scintillator elements within a detector module.

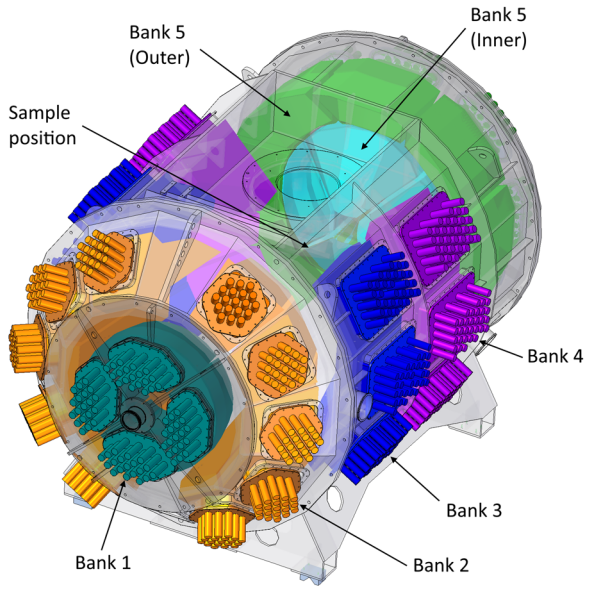

FIG. 5. The arrangement of the detector banks within the Polaris sample tank vacuum vessel. The neutron beam enters the tank from the top right-hand corner of the diagram and exits through the middle of bank 1 in the lower left-hand corner.

with the detectors mounted outside, such that the scattered neutrons must pass through the sample tank (or thin vacuum windows built in to it) after scattering from the sample. However, this approach has a number of drawbacks, including placing restrictions on the shape and size of vacuum windows, which in turn impose constraints on the number of detectors and their locations. For the upgraded Polaris, a radically different approach was chosen in which the detector modules are installed inside a much larger vacuum tank so that there are no windows between the sample and detector, allowing provision of an extremely large solid angle of detector coverage. This has implications for the operation of the detectors because, whilst the ZnS neutron-detecting material and its optical fibers (described in Sec. II E) may be placed in a vacuum, it is impractical to locate the PMTs and their associated electronics, which are an integral component of the detectors, inside the vacuum tank. This issue was resolved by encasing the bundles of fibers within cylindrical blocks of epoxy resin around which vacuum-tight O ring seals could be made, allowing the PMTs to be mounted outside the tank.

The sample tank vessel itself (see Fig. 6) has a total volume of around 20 000 l and is constructed from steel varying in thickness from 30 mm (main cylindrical section) to 48 mm [the large end plate of diameter ~2.65 m housing the high angle (backscattering) detectors and which is also double skinned to prevent deformation under vacuum]. The inside surfaces are coated with panels of neutron absorbing B_4C, whilst collimating and shielding vanes are positioned between the individual detector modules to further reduce background scattering inside the vessel. To minimize air scattering, the sample vessel is evacuated using Leybold Oerlikon Screwline SP-630 and WAU2001 Roots vacuum pumps, giving a combined pumping speed of ~1750 m^3/h and reaching an operational level of better than 10 mbar in ~10 min (and reaching ~5×10^{-2} mbar in

FIG. 6. The "as-delivered" Polaris sample tank. Photograph: STFC.

under 1 h). Venting to atmospheric pressure is done using a dried air supply as moisture can be absorbed into the B_4C shielding material, which would slow the subsequent pump down process.

G. Radial collimator

The sample tank also includes a new design of curved radial collimator, Fig. 7, to define the volume around the sample position viewed by the detectors and reduce unwanted background scattering from surrounding sample environment apparatus. The openings in the collimator match the areas covered by each of the detector banks, with the vanes in each section—which are separated from one another by a 2θ angle of 2°—designed to follow the geometry of the Debye-Scherrer cones. The collimator vanes are constructed from 0.2 mm thick steel, coated with 100 μm of ^{10}B powder, and define a viewable radius of ~2 cm around the sample position, with almost all scattering outside this radius being absorbed. The main cylindrical body of the collimator is constructed from B_4C-containing "S-dough."

H. Beamstop

Neutrons that are not scattered or absorbed by the sample exit the vacuum vessel and travel to the beamstop. The beamstop

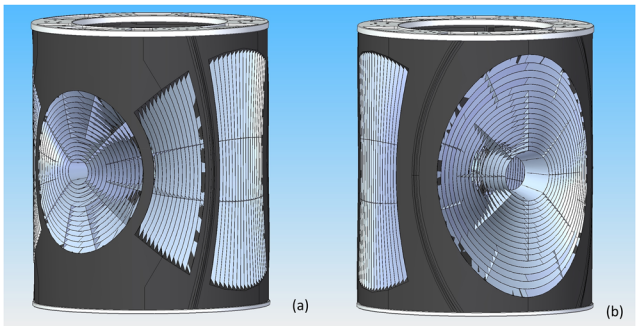

FIG. 7. Schematic illustrations of the Polaris radial collimator (a) viewed from the transmitted beam side, showing collimating vanes for low angle and 90° detector banks (b) viewed from the incident beam side, showing collimating vanes for 90° and backscattering detector banks.

is designed to capture those neutrons reaching it, preventing them from scattering back to the detectors, and ensuring that background radiation levels around the instrument are well below legal radiological limits. It comprises an evacuated flight tube, ~1.2 m long, that transports the transmitted neutron beam into an aluminum container 30 cm square and ~15 cm deep filled with boron carbide powder. Behind this sits 1.2 m of steel; and this is all surrounded by 5 cm thick borated polythene sheets and then by a further 0.5 m of steel blocks. This whole assembly sits on a 1.5 m thick concrete "raft" and is further surrounded by a number of overlapping borated wax-filled steel tanks, each 30 cm thick.

I. Data acquisition electronics and instrument control

The data acquisition electronics for Polaris can be split into 4 discrete sections, as described below. With the exception of the PhotoMultiplier Tube (PMT) assemblies, these all reside in a dedicated screened room with an Uninterruptable Power Supply (UPS) that combine to eliminate airborne electromagnetic and mains power noise.

(i) 924 PMT assemblies are spread across the 38 detector modules (Sec. II E), each one incorporating a high voltage divider to distribute the stepped voltages to the PMT dynodes and a RAL10 fast discriminator to filter out false triggers (e.g., PMT noise).
(ii) Low voltage (−5 V) distribution electronics distribute power to the RAL10 discriminators.
(iii) Detector interface electronics, which process the signals from the PMTs to discriminate between neutron and gamma events using an analog based chain of electronics. Programmable logic devices at the end of the chain then create a detector module event by using channel coincidence logic, determined by the pair coding of fibers and PMTs described in Sec. II E. Although the Polaris detectors vary in the number of scintillator elements and PMT assemblies per module, the same version of the interface card is used for all of them, with the internal programmable logic configured for the number of tubes and the coding used in each module.
(iv) The Data Acquisition Electronics (DAE) comprises a single crate of ten DAE2 Detector cards (each Detector card has 128 Mbytes of on-board memory and records neutron events from up to four detector modules). The DAE captures both the position of the detector and the time-of-flight of the detected neutron events and stores this information in either of two ways.

For standard histogramming of the data, detected events are counted into one of a large number of time channels covering the 20 ms time frame between successive pulses of neutrons from the ISIS target. Data are accumulated into the time channels for sufficient periods of time (number of neutron pulses) to produce datasets whose counting statistics are appropriate for the experiment being undertaken. On Polaris, the time channel widths across the frame vary in a way that follows the $\Delta d/d$ resolution function of the diffractometer, meaning that all diffraction peaks measured in a single detector element will require the same number of time channels to record their profile regardless of their actual time-of-flight.

An alternative to histogramming is to use Event Mode, whereby the detected events are stored as a list on an ISIS frame-by-frame basis as an Event Mode data packet. The Event Mode packet also includes protons-per-pulse data (representing the intensity of the ISIS neutron beam) and any veto conditions that occurred within the frame (for example, the chopper going out of phase or a temperature drifting out of predefined limits). With Event Mode, an instrument user can decide whether to include or exclude frames with veto conditions after such conditions have occurred. Furthermore, because the incident beam monitors generate many more events per frame than the detectors, a mixed Event Mode/Histogram Mode of DAE operation can be set up with the 14 individual monitor PMT channels having their own dedicated DAE2 Detector card.

A particular advantage of Event Mode is that it enables, for example, a single data set collected over several hours to be split into an arbitrary number of individual data sets—each covering smaller intervals within the longer period—at any time (and reprocessed any number of times) after the data collection has been completed. This is especially useful in following chemical processes, where a single data set collected over the duration of a reaction may subsequently be used to create a number of discrete data sets each covering perhaps only a few minutes, thereby allowing the counting statistics in the data set to be optimized while still maintaining an adequate time resolution to understand the reaction.

All aspects of beamline control and data collection are handled by a single Windows PC (a Windows 7 ×64 Virtual Machine). This computer uses a National Instruments USB connection to communicate with the VMEbus chassis of the DAE. A Moxa NPort Serial port device server converts Ethernet data to Serial data (and vice versa) for communication with equipment using RS232 interfaces (e.g., temperature controllers, sample changers). GPIB and USB interfaces are also available for control of beamline or sample environment apparatus.

J. Software

Two software packages are utilized on the beamline during experiments: one (IBEX) to control all aspects of the data collection and sample environment equipment and a second (Mantid) to process the data and reduce it into a format suitable for, e.g., Rietveld profile refinement.

IBEX is a client-server application which coordinates the activities of a number of software components, each of which controls a separate aspect of an ISIS experiment:

(i) The Instrument Control Program (ICP) controls the DAE, informing it when to start and stop data collection, including automatically suspending data collection temporarily if certain conditions (e.g., sample temperature or pressure or synchronization of the chopper) are not within user-defined limits. The ICP is also responsible for transferring the final data set from the DAE to a file.
(ii) The IBEX server is a collection of cooperating software components, based on the EPICS control-system framework (http://www.aps.anl.gov/epics/). The primary components of the IBEX server are Input-Output Controllers (IOCs) and the Blockserver. The IOCs control sample environment equipment and beamline components, whilst the Blockserver

coordinates the activities of IOCs and other components, including the ICP and a data archiver.

(iii) The IBEX client is a graphical user interface program, which communicates with the IBEX server and provides the primary means by which the experimenter can interact with the components of the IBEX server and the ICP to monitor and control an experiment. The IBEX client also provides a simple scripting environment for running genie_python scripts (see below).

(iv) LabVIEW (National Instruments—http://www.ni.com/en-gb/shop/labview.html) is a visual programming language designed to produce programs, called Virtual Instruments (VIs), for controlling hardware such as sample environment equipment and beamline components. VIs are used to control equipment for which no EPICS driver is available. IBEX uses an in-house designed interface layer to communicate with VIs.

(v) genie_python is an ISIS in-house library of Python (https://www.python.org/) commands which permit the automation of an experiment, enabling, for example, unattended overnight data collection from a sample at a number of temperatures in a furnace or cryostat or from a number of samples in a sample changer.

K. Instrument calibration

Instrument calibration and data normalization and reduction are performed using the Mantid software package[11]—an open source framework created to manipulate, analyze, and visualize neutron scattering data.

Initial calibration of the detector banks is a 2-stage process. Based on a geometric description of the detector arrangement (using "ideal" flight paths and scattering angles derived from engineering drawings), the Mantid *AlignDetectors* algorithm does an initial conversion of the data into *d*-spacing from the time-of-flight units of the collected data. Because the actual detector geometry achieved during construction and installation of the diffractometer inevitably differed slightly from this ideal layout, small offsets need to be applied to the converted *d*-spacings in order to achieve the final "focusing" of the data. These offsets were determined using the Mantid *CrossCorrelate* algorithm: an arbitrary reference detector element was chosen and a cross correlation function was calculated between it and the data in each of remaining elements, with the maximum in this function for each detector giving the shift in the *x*-axis position (positive or negative) required to put all the detectors on the same *d*-spacing scale.

L. Data normalization and reduction

Normalization of time-of-flight diffraction data entails accounting for the fact that both the intensity of the incident polychromatic ("white") neutron beam and the efficiency of the ZnS scintillator in the detectors vary as a function of wavelength. These combined effects can be quantified by measuring an isotropically scattering sample, such as vanadium: for this purpose, a 5 mm diameter vanadium rod is used on Polaris. The data from the vanadium rod first have an empty diffractometer (i.e., no sample) data set subtracted to account for the sample independent instrument background, before being corrected for wavelength-dependent absorption effects (with the Mantid *CylinderAbsorption* algorithm) and finally are smoothed to remove the (very weak) Bragg reflections present (using the Mantid *SplineBackground* algorithm).

Once focused and normalized, the resulting 5 powder diffraction patterns (one for each of the Polaris detector banks) are stored in a Mantid workspace from where they may be written to files suitable for input to common Rietveld refinement packages, e.g., Fullprof,[12] EXPGUI+GSAS,[13] or Topas.[14]

III. SELECTED SCIENTIFIC EXAMPLES

The first data sets collected during the commissioning of the upgraded Polaris instrument demonstrated that the performance of the new diffractometer, and, in particular, the improvements in count rate and $\Delta d/d$ resolution, were consistent with that predicted by the Monte Carlo simulations. This is illustrated in Fig. 8 for the case of the dramatically increased count rate in the detector banks at low scattering angles and improved resolution at backscattering angles. However, the major scientific driver for the instrument upgrade was to perform neutron powder diffraction experiments that were not previously possible on Polaris. So, rather than focus in detail on the relative performance of the old and new instruments, we highlight a number of recent scientific studies which demonstrate the capabilities of the new instrument.

A. Small sample volumes

The increased count rate afforded by the large area detectors on the upgraded Polaris allows the collection of high quality data from significantly smaller sample sizes than those typically associated with

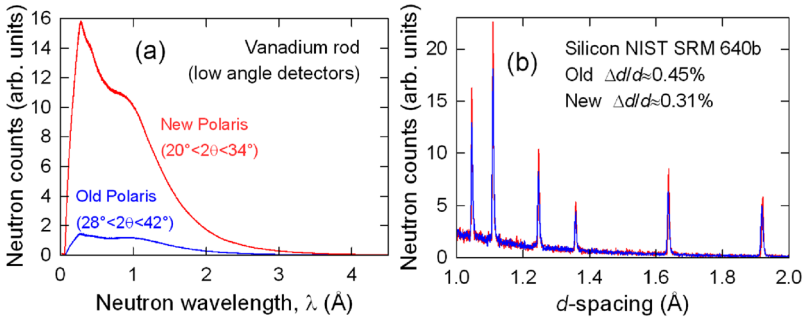

FIG. 8. Illustration of (a) the increase in neutron count rate (normalized to data acquisition period) in the detector banks at low scattering angles (Old: 28° < 2θ < 42°; Upgrade: 19° < 2θ < 34°). (b) The improved $\Delta d/d$ resolution at backscattering angles (Old: 130° < 2θ < 160°; Upgrade: 146° < 2θ < 167°).

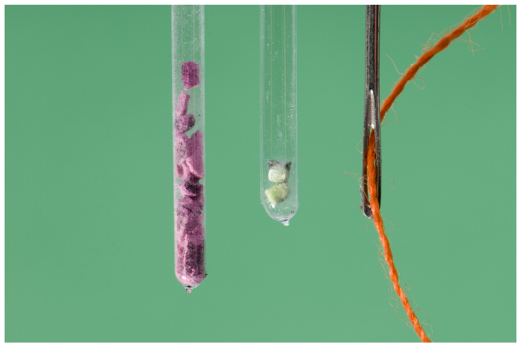

FIG. 9. Photograph of the samples of $NaCoF_3$ (left) and $NaNiF_3$ (right) postperovskite samples used for the neutron powder diffraction experiments on the upgraded Polaris. The diameter of the silica glass capillary tubes in which the sample is contained is 1.5 mm. Reproduced with permission from Lindsay-Scott *et al.*, J. Appl. Crystallogr. **47**, 1939 (2014). Copyright 2014 International Union of Crystallography. Photograph: STFC.

neutron powder diffraction studies. This is illustrated by a study of the postperovskite phases of $NaCoF_3$ and $NaNiF_3$.[15] These materials are structural analogs to the postperovskite phase of $MgSiO_3$, believed to be a major component of the D'' region in the Earth's mantle.[16] The synthesis of these samples under conditions of high temperature and pressure in multi-anvil presses means that only very small amounts can be prepared (~50 mg or less in this case, see Fig. 9). Nevertheless, high quality neutron powder diffraction data were collected from these two samples, from which accurate structural parameters could be obtained by Rietveld profile refinement (see Fig. 10). This enabled the detailed geometries of the CoF_6 and NiF_6 octahedra and the tilt angles between them to be determined with much better accuracy and precision than is possible using X-ray diffraction, thereby providing important information for understanding geological processes occurring in the Earth's mantle. Furthermore, inspection of the refined structural parameters and their estimated standard deviations obtained from data sets collected for progressively increasing periods of time between 1 and 48 h during this study showed that ~6 h was sufficient data collection time for these extremely small samples. The longer collection times yielded negligible differences in the values of the refined parameters and no further improvement in the estimated standard deviations (for further details, see the Electronic Supplementary Information to the paper by Lindsay-Scott *et al.*[15]).

B. Time resolved studies

Where larger quantities of sample are available, the high count rate achieved using large area detectors permits data collection in very short periods of time, typically a few minutes or less. Combined with the penetrating properties of neutrons, which facilitates the collection of diffraction patterns from samples contained in bulky reaction cells, this enables complex chemical reactions to be studied in real time.

A time-resolved neutron powder diffraction study followed the regeneration of sodium alanate ($NaAlD_4$), formed when activated NaD reacts with D_2 gas at 100 °C. With the reaction taking place at a pressure of 100 bars, the sample was contained in a thin-walled aluminum alloy pressure cell (internal diameter 7 mm, wall thickness 0.75 mm), but even with a relatively small sample volume of ~1 cm^3, data sets collected in just 3 min intervals produced diffraction patterns of sufficient quality to determine the phase composition of the sample throughout the reaction, showing how Na_3AlD_6 is formed initially, which then reacts further to produce $NaAlD_4$ (see Fig. 11).[17]

This experiment was motivated by the need to understand the kinetics of hydrogen storage within solid media as this is essential to identify viable long-term replacements to fossil fuel power generation. Indeed, studies of the structure-property relationships within materials of relevance for energy production and storage have formed a major component of the science programme on Polaris

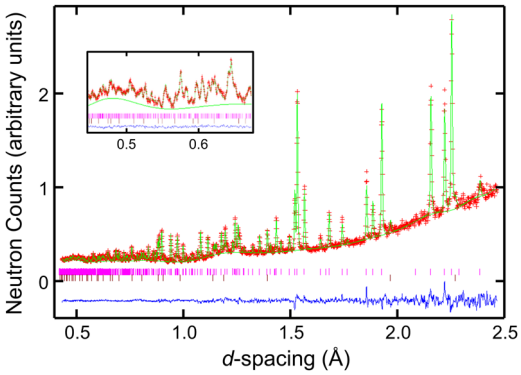

FIG. 10. Observed (points), calculated (line), and difference (lower trace) neutron powder diffraction patterns for Rietveld refinements with data collected on the upgraded Polaris diffractometer (bank 5) from $NaCoF_3$. The inset diagram shows the region $0.445 < d$ (Å) < 0.66 in greater detail. The rise in the background as the d-spacing increases is due to scattering from the silica glass capillary tubes used to contain the sample. Reproduced with permission from Lindsay-Scott *et al.*, J. Appl. Crystallogr. **47**, 1939 (2014). Copyright 2014 International Union of Crystallography.

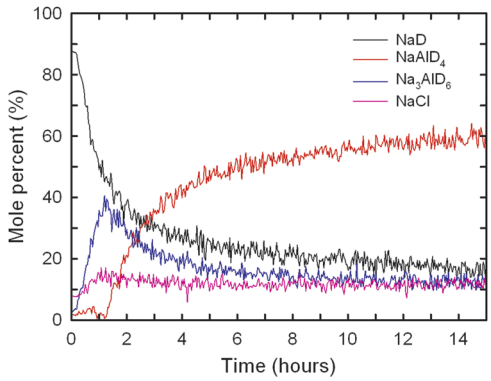

FIG. 11. The mole percent of various crystalline phases observed as a function of time as determined using neutron powder diffraction data collected on Polaris. Under the D_2 atmosphere, NaD is gradually converted to Na_3AlD_6 and then to $NaAlD_4$. NaCl is included as a spectator phase. Reproduced with permission from Humphries *et al.*, J. Mater. Chem. A **2**, 16594 (2014). Copyright 2014 The Royal Society of Chemistry.

since its upgrade, reflecting the technological importance of new compounds for use within battery and fuel cell applications. The majority of these materials are characterized by mobile H^+, Li^+, and O^{2-} ions within a solid containing heavier elements, so the study of the structural and diffusion properties is well suited to neutron diffraction methods. Further examples are given below.

C. *In situ* studies of batteries

As part of a collaborative project between ISIS and the University of Stockholm, an electrochemical cell has been developed to enable the structural changes occurring in battery electrode materials to be probed *in situ* during charging and discharging in the neutron beam on Polaris. The design of the cell, shown in Fig. 12, can be considered to be an enlarged version of a typical commercial lithium-ion coin cell, although of a highly modular construction to allow different choices of current collector and separator, or to allow a number of cells to be mounted in series in order to maximize the amount of material in the neutron beam (hence increase the count rate and reduce the time required to collect individual data sets). Full details of the cell can be found elsewhere.[18]

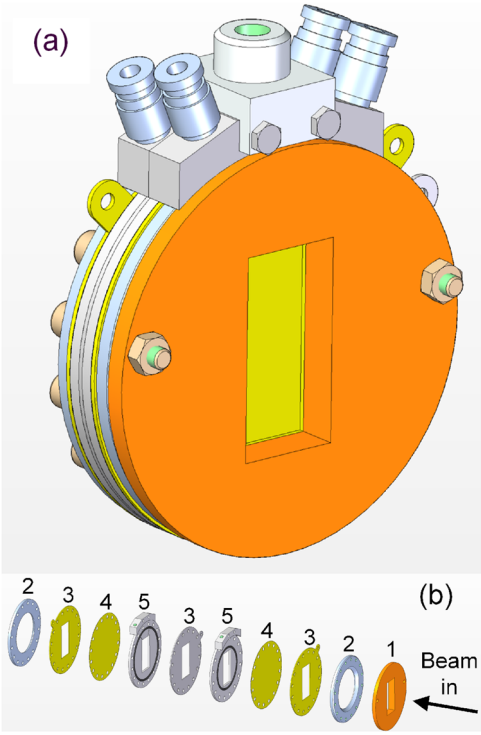

FIG. 12. The cell built to enable studies of battery materials *in situ* during electrochemical experiments. (a) a CAD image of the assembled cell and (b) an exploded view of the cell components and their positions with respect to the incident neutron beam: (1) the boron nitride shield, (2) stainless steel clamp rings, (3) nickel window, (4) thin nickel metal sheet (also acts as current collector), and (5) polymer separator. The assembly is clamped together using nuts and bolts manufactured from PEEK (polyether ether ketone), visible in (a). Reproduced with permission from Biendicho *et al.*, J. Power Sources **248**, 900–904 (2014). Copyright 2014 Elsevier.

As an example of its use, the electrochemical reactions at both the positive and negative electrodes of a nickel metal hydride (Ni-MH) battery during charging have been studied *in situ*. Commercially available β-$Ni(OH)_2$ and $LaNi_5$-based powders were used as the positive and negative electrodes, respectively, with the former converted first to β-$Ni(OD)_2$ by exchanging hydrogen with deuterium via *ex situ* cycling of the cell prior to the *in situ* measurements. Neutron diffraction data collected as a series of datasets, each of 30 min duration, show a large solid solution domain for the positive β-$Ni(OD)_2$ electrode, as well as an increase in the (110) peak width, during charge (see Fig. 13).[19] The cell is now being used, in a slightly modified form, to probe the structural properties of lithium battery materials on Polaris.[20]

D. Gas flow cell

In a complementary development linked to the instrument upgrade project, a gas flow cell has been built[21] to study materials under various controlled gas atmospheres (static, flowing, and/or variable composition). This allows experiments to be performed in which the sample can be subjected to conditions which closely mimic those found in real technological applications, e.g., to investigate structural changes in a solid oxide fuel cell (SOFC) electrolyte as a function of oxygen gas pressure.[22]

A recent structural investigation in a related field, focused on understanding the oxygen decoupling and uptake mechanism of bixbyite, $(Fe, Mn)_2O_3$, at temperatures where it is used as a material for chemical looping with oxygen uncoupling (CLOU).[23] CLOU is a method currently under development that will allow efficient CO_2 capture during fuel combustion in a power plant. The process involves transporting oxygen from an air reactor to a fuel reactor using a solid oxygen carrier, thereby keeping the CO_2 and H_2O (which may be removed by condensation) formed from the other gases present in the system (N_2 and O_2) and eliminating the need

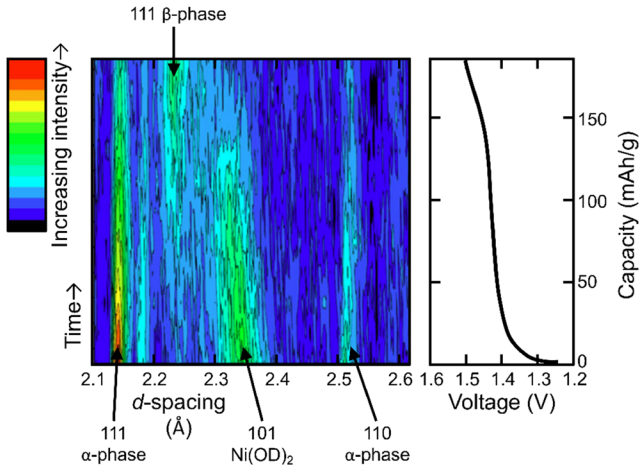

FIG. 13. Color map showing structural changes at both positive and negative electrodes in a Ni–MH battery as a function of charge and the voltage profile vs capacity for the cell measured *in situ*. Reproduced with permission from Biendicho *et al.*, J. Mater. Res. **30**(3), 407–416 (2015). Copyright 2015 Cambridge University Press.

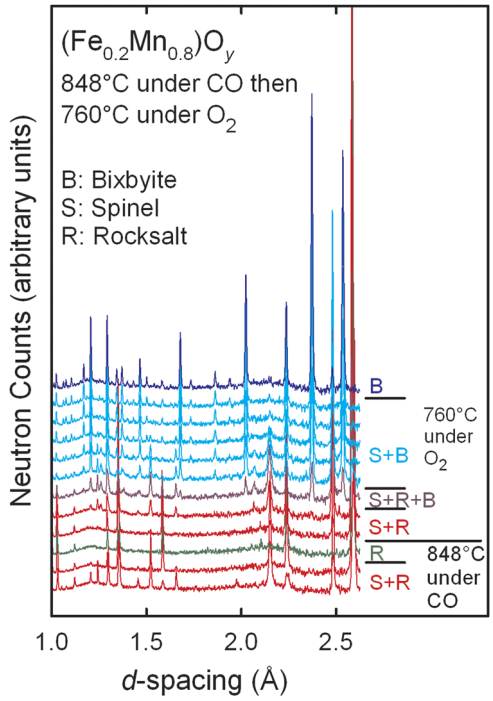

FIG. 14. The evolution of a portion of the neutron powder diffraction pattern from $(Fe_{0.2}Mn_{0.8})_2O_3$ heated under CO at 848 °C showing the formation of the rocksalt (R) structured phase and the subsequent reforming of the spinel (S) and bixbyite (B) structured phases at 760 °C under O_2. Reproduced with permission from Norberg *et al.*, CrystEngComm **18**, 5537 (2016). Copyright 2016 The Royal Society of Chemistry.

for energy consuming and costly gas separation. Analysis of *in situ* neutron diffraction data collected between 700 and 1000 °C under constant oxygen partial pressure revealed detailed information concerning the phase changes which facilitate oxygen release and oxygen uptake in bixbyite, via the reactions M_2O_3 (bixbyite) ↔ M_3O_4 (spinel) ↔ MO (rocksalt), M = $(Fe_{0.2}Mn_{0.8})$ (see Fig. 14).[24]

E. Total scattering studies

Total scattering is a technique in which the Bragg and diffuse scattering in a powder diffraction pattern is measured and analyzed simultaneously. The total scattering function, $S(Q)$, is generated from the raw data through careful normalization and background subtraction and is then commonly Fourier transformed to produce a pair distribution function, $G(r)$ (often referred to simply as the PDF), which can be thought of as a histogram, weighted by both scattering power and coordination number, of pairwise interatomic distances (Fig. 15). Each "peak" in an experimental PDF corresponds to one or more distances at which pairs of atoms are found in the structure. For example, consider the structure of SiO_2 which consists of a network of $[SiO_4]$ tetrahedral units. The first peak in the PDF is at about 1.6 Å and corresponds to the Si—O bond, the second peak represents the distance between 2 oxygen atoms across the edge of a tetrahedron, the third peak represents the distance between silicon atoms in neighboring tetrahedra, and so on. Structural information may be extracted from a PDF in a variety of ways, such as straightforward inspection, simple peak fitting, small-box "Rietveld-like" modeling using a crystal structure, or big-box modeling using reverse Monte Carlo (RMC) methods. Regardless of which method (or combination of methods) is used, analysis of the PDF is, by definition, biased toward local rather than long-range structural features and provides a unique view of complex and/or disordered systems, which has proven to be extremely important when attempting to understand many important functional materials.[25–30]

A total scattering measurement differs from a more typical powder diffraction measurement in several ways:

(i) Data must have high statistical quality, particularly in the high-Q (low d-spacing) region. This generally necessitates longer collection times.
(ii) Data must also be collected from the empty instrument as well as any sample environment and the container to allow for accurate corrections to be applied.
(iii) For normalization and corrections to be done accurately, sample containers should be chosen to ensure that the depth of sample in the container is greater than the height of the incident neutron beam. Generally, this will be achieved by reducing the diameter of the container, but where this is not possible (e.g., solid metal ingot samples or very small sample quantities), the height of the incident neutron beam should be reduced using collimation.

The upgraded Polaris instrument is ideal for total scattering measurements for several reasons: its fast count rate and low instrumental background maximizes data quality, the wide

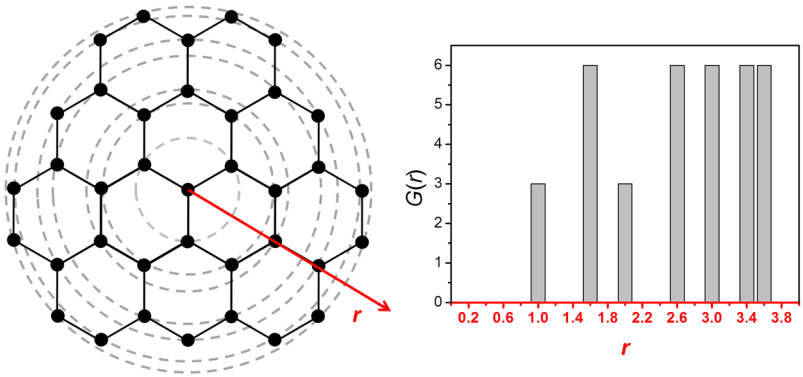

FIG. 15. The construction of a pair distribution function (PDF) for a simple 2D array. Conceptually, an atom is placed at the origin and its neighbors counted as a function of distance, r. This is then repeated for every atom in the array to produce the summed histogram, where a peak is found at every occupied distance (shown as dashed lines).

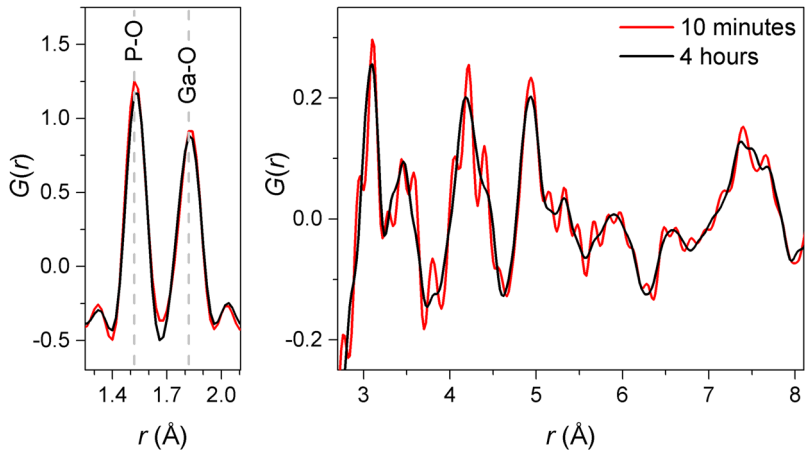

FIG. 16. Example total scattering datasets measured on Polaris from quartz-type $GaPO_4$.

angle detector coverage provides a large accessible Q-range (Q_{max} ~ 50 Å^{-1}, or ~0.13 Å in d-spacing), and its good reciprocal space resolution produces PDFs which do not suffer from major instrumental damping.

Quartz-type SiO_2 is one of the most commercially important piezoelectric materials in use today, but degradation of its piezoelectric behavior at high temperature limits its application in some fields. The apparently isostructural $GaPO_4$ analog benefits from superior temperature stability, which a series of total scattering experiments[31] have attributed to the stability of its atomic structure on a local level. Example total scattering datasets from a sample of $GaPO_4$ are shown in Fig. 16. The first peaks in the PDF can be assigned to P—O and Ga—O bonds, the third is due to nearest-neighbor O—O correlations, and so on. In this way, an intuitive understanding of the local structure of the material can be obtained through simple inspection of the PDF. $GaPO_4$ serves as an ideal standard for assessing the capabilities of Polaris, both because of its industrial relevance and because the difference in size of the [GaO_4] and [PO_4] tetrahedra is well established through analysis of Bragg diffraction data. The two datasets in Fig. 16 differ by counting time: one was collected for ~10 min and the other for ~4 h. The reduction in high-frequency noise in the longer-duration dataset is obvious. Surprisingly, the splitting of the P—O and Ga—O peaks is clearly visible even in the ~10 min dataset and the effect of increased high-Q noise on the low-r region of the transform is minimal. The mid-r range, however, is severely affected by this noise and this may limit the use of such data for modeling purposes.

These results highlight the unprecedented ability of Polaris to perform "time-resolved" total scattering measurements, something which has traditionally been thought to be far outside the realm of possibility. The incredibly high intensity of synchrotron X-ray sources make beamlines like the XPDF at the Diamond Light Source or 11-ID-B at APS the only route for obtaining truly rapid PDF data, nevertheless the complementarity of X-ray and neutron measurements is well understood and is only enhanced by the performance of Polaris in these tests.

IV. GLOBAL CONTEXT

In the period from the conception of the Polaris upgrade in around 2006 to its completion in 2012, several other neutron powder diffraction facilities were developed around the world. The Japanese spallation source J-PARC and the new Spallation Neutron Source (SNS) in the USA both came online; whilst the European spallation source (ESS) was given the go-ahead and is now under construction. In this context, it is useful to look at where the new Polaris instruments fits into this global landscape of neutron scattering.

Major developments in neutron sources have been predominantly focused on spallation facilities, and the intrinsic advantages of short pulse sources are being exploited by the development of high intensity powder diffractometers such as POWGEN at the SNS and NOVA at J-PARC. Looking to the future, the ESS facility will exploit a broad pulse to generate a high flux of neutrons and will then utilize choppers close to the source to mimic shorter pulses and achieve adequate $\Delta d/d$ resolution on instruments such as DREAM and HEIMDAL. This has the advantage that, by tuning the opening window, it is possible to trade between resolution and count rate to optimize the instrument performance for a given experiment. However, using a chopper system which defines a Δt that is constant for all wavelengths (rather than the essentially constant $\Delta t/t$ provided by short pulse spallation sources such as ISIS), it will be difficult to achieve high resolution at low d-spacings (high Q). Perhaps more importantly, the lower flux of epithermal neutrons available at the ESS will limit the high Q achievable for PDF studies to below around 20 Å^{-1}, which restricts the real space resolution. In this context, it is interesting to note that the total scattering research program on Polaris is growing rapidly (in the 3 years leading up to the upgrade total scattering experiments only accounted for 19% of experiments, whereas since the science programme resumed on the upgraded instrument, this has risen to ~50%), and touches on many of the key scientific areas identified above, such as batteries to engineering materials, photovoltaics, oxygen conducting membranes for use in fuel cells, catalysts, and many more.

Considering, finally, the powder diffractometers at the ISIS neutron facility, Polaris and GEM are its two medium resolution, general purpose instruments. Both have large detector banks (approaching 2π sr detector coverage) and similar $\Delta d/d$ resolutions. However, because they view different moderators, their science programmes have difference emphases, in particular, for total scattering studies involving pair distribution function (PDF) calculations. The incident flux on Polaris from the ambient temperature water

moderator is rich in shorter wavelength neutrons and has a narrow pulse structure making it ideally suited to studying local structures of predominantly crystalline materials—where the good reciprocal space resolution in the data results in high real space resolution in the PDF. The 110 K liquid methane moderator viewed by GEM,[9] however, produces a flux distribution shifted to longer wavelengths and having a slightly broader pulse width. Consequently, total scattering experiments on GEM are more suited to amorphous materials, where structural correlations over longer length scales are more important. Furthermore, the higher flux of long wavelength neutrons improves the counting statistics of the diffraction data at longer d-spacings and means that studies of magnetic materials are done better on GEM.

For ultrahigh resolution powder diffraction experiments at ISIS, HRPD ($\Delta d/d$ resolution $\sim 5 \times 10^{-4}$) is used in experiments involving, e.g., *ab initio* structure determination, unit cell confirmation or studies of subtle phase transitions. Due to its long (~100 m) flight path, HRPD only uses 1 pulse of neutrons in 5 from ISIS target station 1 and as a consequence its count rate—although enhanced at longer wavelengths by the use of a neutron guide in the incident beamline—is significantly lower than that of Polaris and GEM. Nevertheless, the resulting extremely sharp Bragg reflections measured in its backscattering detector bank can have a very high peak:background ratio and means data sets may be collected in relatively short periods of time.

Although studies of materials under high pressures (up to 20 GPa) may be done on Polaris, at ISIS these experiments are almost exclusively carried out using the dedicated infrastructure on the PEARL high pressure instrument.[35] Viewing the same cryogenic moderator as GEM, the incident flux on PEARL is rich in longer wavelength neutrons, which compensates for the increased attenuation of the beam as it passes through the anvils of the Paris-Edinburgh press and ensures that the longer d-spacing Bragg reflections have good counting statistics.

For studies of complex magnetic materials (e.g., incommensurate structures), WISH is the instrument of choice.[34] A supermirror guide transports neutrons from the ISIS second target station solid methane moderator to the sample position to maximize the flux of longer wavelength neutrons, and adjustable collimation in the incident beamline allows the beam size and divergence to be tailored to the sample size to optimize the resolution and count rate for each experiment. Furthermore, the detector design on WISH enables it to study materials in both powder and single crystal form.

V. CONCLUSIONS

In every aspect, the upgraded Polaris instrument has met (or exceeded) the aims and expectations set by the original upgrade criteria. The count rate has been maximized with a ~7-fold increase in total detector solid angle coverage over that of the diffractometer it replaced. The instrumental resolution has been improved with $\Delta d/d$ decreasing from 0.45% to 0.31% at backscattering angles; and finally instrumental backgrounds have been minimized through an innovative advanced sample tank and radial collimator design. This, together with the example results presented above and the large number of successful experiments performed since Polaris resumed operation in March 2012, shows that the instrument upgrade has been highly successful.

The upgrade to the Polaris powder diffractometer at ISIS has had a major impact in the area of "routine" structural studies, allowing more rapid characterization of a diverse range of materials as a function of, e.g., temperature or gas environment, and also during chemical reactions using Rietveld refinement methods. However, the upgrade has also extended the range of scientific studies that can be performed using neutron powder diffraction into new, expanding areas, such as total scattering studies of disordered crystalline materials and *in situ* and *in operando* investigations of chemical and electrochemical reactions. A key component of these advances are the developments of novel sample environment devices, such as *in situ* cells that allow the structural properties of battery materials to be probed during charge-discharge cycling, and *in situ* heating in controlled gas environments. In addition, a reactor using microwave heating to carry out chemical reactions and a cell using microwaves to probe the dielectric properties of solid state materials during gas uptake are also in development on Polaris.[32] The continued development of software for total-scattering data analysis, such as RMCProfile,[33] both benefits from and is of benefit to the scientific expansion, with far more complex problems being investigated than has been possible in the past. It is anticipated that the scope of research brought to Polaris will continue to expand in future to fully exploit its new capabilities.

ACKNOWLEDGMENTS

The authors would like to acknowledge the vital contribution made to this work by the late Professor Sten Eriksson (Chalmers University of Technology, Gothenburg, Sweden) who—as the holder of grants from the Vetenskapsrådet Research Council funding both the Swedish financial contribution to the ISIS Neutron and Muon Source and the postdoctoral research project of Dr. S. T. Norberg—would have been included as a co-author of this paper were it not for his untimely death before the manuscript was submitted.

The Polaris upgrade project was funded by the CCLRC/STFC Facilities Development Fund, with additional financial contributions from the Swedish Vetenskapsrådet Research Council and in-kind support from The Basque Country, Spain (project led by Professor J. Bermejo). The design and construction of the instrument greatly benefitted from significant scientific, technical, and financial input from a number of collaborators, including members of the project's Scientific Advisory Committee—Anthony Powell (University of Reading, chair), Paolo Radaelli (University of Oxford), Brian Holsman (ISIS), Colin Pulham (University of Edinburgh), Neil Hyatt (University of Sheffield), Paul Schofield (Natural History Museum, London), and Simon Clarke (University of Oxford). The design and installation of the upgraded Polaris was a major project, made possible by the efforts of numerous staff within the ISIS Electrical Engineering Group, the ISIS Mechanical Engineering Group, the ISIS Instrument Design Group, the ISIS Electrical Design Group, the ISIS Computing Group, the ISIS Electronics Group, the ISIS Detector Group, the ISIS Sample Environment Group, the ISIS Instrument Operations Group, and the Electrical and Electronic User Support Group. The authors are grateful to Ian Wood (University College London), Josh Makepeace (University of Oxford), Bill David (ISIS), Jordi Jacas Biendicho (IREC, Barcelona), and Henrik Leion (Chalmers University) for permitting the use of their research results in this paper.

REFERENCES

[1]W. I. F. David, W. T. A. Harrison, J. M. F. Gunn, O. Moze, A. K. Soper, P. Day, J. D. Jorgensen, D. G. Hinks, M. A. Beno, L. Soderholm, D. W. Capone, I. K. Schuller, C. U. Segre, K. Zhang, and J. D. Grace, Nature **327**, 310 (1987).

[2]P. G. Radaelli, D. E. Cox, M. Marezio, and S. W. Cheong, Phys. Rev. B **55**, 3015 (1997).

[3]W. I. F. David, R. M. Ibberson, J. C. Matthewman, K. Prassides, T. J. S. Dennis, J. P. Hare, H. W. Kroto, R. Taylor, and D. R. M. Walton, Nature **353**, 147 (1991).

[4]A. R. Armstrong, M. Holzapfel, P. Novak, C. S. Johnson, S. H. Kang, M. M. Thackeray, and P. G. Bruce, J. Am. Chem. Soc. **128**, 8694 (2006).

[5]W. F. Kuhs, J. L. Finney, C. Vettier, and D. V. Bliss, J. Chem. Phys. **81**, 3612 (1984).

[6]S. Hull, R. I. Smith, W. I. F. David, A. C. Hannon, J. Mayers, and R. Cywinski, Physica B **180**, 1000 (1992).

[7]J. M. Besson, R. J. Nelmes, G. Hamel, J. S. Loveday, G. Weill, and S. Hull, Physica B **180**, 907 (1992).

[8]S. Hull, W. I. F. David, and M. W. Johnson, in *Measurement of Residual and Applied Stress Using Neutron Diffraction*, Nato Advanced Science Institutes Series, Series E, Applied Sciences Vol. 216, edited by M. T. Hutchings and A. D. Krawitz (Kluwer Academic Publishing, Dordrecht, 1992), p. 383.

[9]A. C. Hannon, Nucl. Instrum. Methods Phys. Res., Sect. A **551**, 88 (2005).

[10]P. Willendrup, E. Farhi, and K. Lefmann, Physica B **350**, E735 (2004).

[11]O. Arnold, J. C. Bilheux, J. M. Borreguero, A. Buts, S. I. Campbell, L. Chapon, M. D. N. Draper, R. Ferraz Leal, M. A. Gigg, V. E. Lynch, A. Markvardsen, D. J. Mikkelson, R. L. Mikkelson, R. Miller, K. Palmen, P. Parker, G. Passos, T. G. Perring, P. F. Peterson, S. Ren, M. A. Reuter, A. T. Savici, J. W. Taylor, R. J. Taylor, R. Tolchenov, W. Zhou, and J. Zikovsky, Nucl. Instrum. Methods Phys. Res., Sect. A **764**, 156 (2014).

[12]J. Rodriguez-Carvajal, Physica B **192**, 55 (1993).

[13]B. H. Toby, J. Appl. Crystallogr. **34**, 210 (2001).

[14]A. A. Coelho, J. S. O. Evans, I. R. Evans, A. Kern, and S. Parsons, Powder Diffr. **26**, S22 (2011).

[15]A. Lindsay-Scott, D. Dobson, F. Nestola, M. Alvaro, N. Casati, C. Liebske, K. S. Knight, R. I. Smith, and I. G. Wood, "Time-of-flight neutron powder diffraction with milligram samples: The crystal structures of $NaCoF_3$ and $NaNiF_3$ post-perovskites," J. Appl. Crystallogr. **47**, 1939 (2014).

[16]D. P. Dobson, S. A. Hunt, A. Lindsay-Scott, and I. G. Wood, Phys. Earth Planet. Inter. **189**, 171 (2011).

[17]T. D. Humphries, J. W. Makepeace, S. Hino, W. I. F. David, and B. C. Hauback, "Regeneration of sodium alanate studied by powder *in situ* neutron and synchrotron X-ray diffraction," J. Mater. Chem. A **2**, 16594 (2014).

[18]J. J. Biendicho, M. Roberts, C. Offer, D. Noreus, E. Widenkvist, R. I. Smith, G. Svensson, K. Edstrom, S. T. Norberg, S. G. Eriksson, and S. Hull, "New *in situ* neutron diffraction cell for electrode materials," J. Power Sources **248**, 900–904 (2014).

[19]J. J. Biendicho, M. Roberts, D. Noreus, U. Lagerqvist, R. I. Smith, G. Svensson, S. T. Norberg, S. G. Eriksson, and S. Hull, "*In situ* investigation of commercial $Ni(OH)_2$ and $LaNi_5$-based electrodes by neutron powder diffraction," J. Mater. Res. **30**(3), 407–416 (2015).

[20]B. Dong, J. J. Biendicho, S. Hull, R. I. Smith, and A. R. West, J. Electrochem. Soc. **165**, A793 (2018).

[21]R. Haynes, S. T. Norberg, S. G. Eriksson, M. A. H. Chowdhury, C. M. Goodway, G. D. Howells, O. Kirichek, and S. Hull, J. Phys.: Conf. Ser. **251**, 012090 (2010).

[22]M. Burbano, S. T. Norberg, S. Hull, S. G. Eriksson, D. Marrocchelli, P. A. Madden, and G. W. Watson, Chem. Mater. **24**, 222 (2012).

[23]T. Mattisson, A. Lyngfelt, and H. Leion, Int. J. Greenhouse Gas Control **3**, 11 (2009).

[24]S. T. Norberg, G. Azimi, S. Hull, and H. Leion, "*In situ* neutron powder diffraction study of the reaction $M_2O_3 \leftrightarrow M_3O_4 \leftrightarrow MO$, M = $(Fe_{0.2}Mn_{0.8})$: Implications for chemical looping with oxygen uncoupling," CrystEngComm **18**, 5537 (2016).

[25]H. Y. Playford, L. R. Owen, I. Levin, and M. G. Tucker, Annu. Rev. Mater. Res. **44**, 429 (2014).

[26]M. T. Dove, M. G. Tucker, and D. A. Keen, Eur. J. Mineral. **14**, 331 (2002).

[27]C. A. Young and A. L. Goodwin, J. Mater. Chem. **21**, 6464 (2011).

[28]S. J. L. Billinge and I. Levin, Science **316**, 561 (2007).

[29]H. Playford, D. Keen, and M. Tucker, Neutron News **27**, 17 (2016).

[30]S. J. L. Billinge and T. Egami, *Underneath the Bragg Peaks: Structural Analysis of Complex Materials* (Pergamon, Oxford, 2003), Vol. 16.

[31]J. Haines, O. Cambon, N. Prudhomme, G. Fraysse, D. A. Keen, L. C. Chapon, and M. G. Tucker, Phys. Rev. B **73**, 014103 (2006).

[32]M. O. Jones, J. Hartley, and A. Porch, Phys. Chem. Chem. Phys. **18**, 23340 (2016).

[33]M. G. Tucker, D. A. Keen, M. T. Dove, A. L. Goodwin, and Q. Hui, J. Phys.: Condens. Matter **19**, 335218 (2007).

[34]L. C. Chapon, P. Manuel, P. G. Radaelli, C. Benson, L. Perrott, S. Ansell, N. J. Rhodes, D. Raspino, D. Duxbury, E. Spill, and J. Norris, Neutron News **22**, 22–25 (2011).

[35]C. L. Bull, N. P. Funnell, M. G. Tucker, S. Hull, D. J. Francis, and W. G. Marshall, High Pressure Res. **36**, 493–511 (2016).